

Article

Chip Morphology and Surface Integrity in Turning AZ31 Magnesium Alloy under Dry Machining and Submerged Convective Cooling

Muhammad Syamil Zakaria ^{1,2,*} , Mazli Mustapha ¹, Azwan Iskandar Azmi ²  and Chu Yee Khor ^{2,*} 

¹ Department of Mechanical Engineering, Universiti Teknologi PETRONAS, Seri Iskandar 32610, Perak, Malaysia

² Department of Manufacturing, Faculty of Mechanical Engineering & Technology, Pauh Putra Campus, Universiti Malaysia Perlis, Pauh 02600, Perlis, Malaysia

* Correspondence: syamil@unimap.edu.my (M.S.Z.); cykhor@unimap.edu.my (C.Y.K.)

Abstract: Magnesium alloys have broad applications, including medical implants and the aerospace sector owing to their great density and high strength-to-weight ratio. Dry cutting is a frequent technique for machining this material. However, it always leads to an excessive rise in temperature due to the absence of cooling at the cutting zone, which affects the machined surface integrity and chip morphology. In this study, chip morphology and surface integrity of the AZ31 magnesium alloy were investigated in the turning process using an internal cooling method called submerged convective cooling (SCC) to overcome the absence of cooling in dry cutting. This method can exploit the advantage of the high specific heat capacity of water as a cooling fluid without any reaction between water and magnesium to create a cooling element in the cutting zone. The chip morphologies and surface integrity were analyzed experimentally with varying cutting speeds under SCC and dry cutting. The experimental results revealed that SCC and dry cutting produced saw-tooth or serrated chip formation. The chips produced in dry cutting were continuous, while SCC was short and discontinuous as a result of a severe crack on the back surface of the chip. It was discovered that the grain refinement layer on the machined samples was thinner under SCC turning. SCC machining increased the microhardness of the AZ31 magnesium alloy by 60.5% from 55 HV to 88.3 HV, while dry turning exhibited a 49% increase in microhardness. The result revealed that surface roughness improved by 10.8%, 9.4% and 4.7% for cutting speeds (V) of 120, 180, and 240 m/min, respectively, under the SCC internal cooling. Based on the result obtained, SCC cutting outperformed dry cutting in terms of chip breakability, grain refinement, microhardness, and surface roughness.

Keywords: chip morphology; surface integrity; internal cooling; magnesium alloy; dry cutting



Citation: Zakaria, M.S.; Mustapha, M.; Azmi, A.I.; Khor, C.Y. Chip Morphology and Surface Integrity in Turning AZ31 Magnesium Alloy under Dry Machining and Submerged Convective Cooling. *Metals* **2023**, *13*, 619. <https://doi.org/10.3390/met13030619>

Academic Editor: Reza Alizadeh

Received: 24 February 2023

Revised: 9 March 2023

Accepted: 14 March 2023

Published: 20 March 2023



Copyright: © 2023 by the authors. Licensee MDPI, Basel, Switzerland. This article is an open access article distributed under the terms and conditions of the Creative Commons Attribution (CC BY) license (<https://creativecommons.org/licenses/by/4.0/>).

1. Introduction

Magnesium alloys such as AZ31 are widely used in cutting-edge applications, including medical implants [1,2] and the aerospace industry [3] due to their excellent density and high strength-to-weight ratio [4]. Magnesium and its alloys possess good machinability, making dry machining a practical option [5,6]. Nonetheless, previous research has shown various risks in machining Mg alloys such as self-ignition and strong reactivity of magnesium and oxygen to produce hydrogen gas, especially in dry cutting and water-based coolant applicants, respectively [7]. The size of the β -Mg₁₇Al₁₂ phase in the magnesium composition was found to affect the ease of self-ignition, leading to chip combustion [8]. Several studies were conducted previously to resolve problems in machining Mg alloys. Yu et al. proposed using a non-aqueous coolant to prevent chip ignition by dissipating heat from the cutting zone [9]. Blanco et al., on the other hand, utilized a sustainable cooling method (minimum quantity of lubricant (MQL), cold compressed air (CCA), and cryogenic machining in drilling Mg-Al and Mg-Ti [10]. The results depicted that MQL and

cryogenic machining produced superior outcomes compared to dry cutting. In another study, a combination of cryogenic and MQL, which is known as CryoMQL, produced lower surface roughness than cryogenic and MQL alone when turning magnesium-based composite. However, cryogenic and CryoMQL resulted in higher cutting force than MQL due to the strain hardening of the work material that was caused by lower temperatures in cryogenic cooling [11]. Turning AZ31 magnesium alloy under cryogenic cooling reduced surface roughness by 56% compared to dry cutting [12]. Dinesh et al. conducted a turning experiment on ZK60 magnesium alloy under cryogenic and dry cutting [13]. Their study revealed that cryogenic turning improved surface roughness by 25% to 40%. Extremely low temperatures from cryogenic cooling demonstrated an excellent surface finish in turning AZ31 magnesium alloy. The strong adhesive effect between tools and magnesium was eliminated compared to dry cutting [14]. In another study, Dinesh et al. investigated the effect of dry and cryogenic conditions on the orthogonal cutting of the same alloy. They found a comparable increase in surface roughness on the sample machined under cryogenic conditions [15]. In addition, Eker et al. observed that surface roughness was significantly better under MQL cutting due to lower cutting temperature and less friction between the tool and work material than dry cutting [16]. A previous study revealed that the surface roughness of AZ91HP improved at lower feed rates and high cutting speeds. However, the depth of cut had a negligible impact on the surface parameters measured [17]. Gao et al. assessed cutting parameters in turning AZ31B and found that surface roughness was most affected by feed rate, followed by the depth of cut and cutting speed [18].

Grain refinement at the subsurface of many materials is caused by the extreme plastic deformation that occurs during machining, including nickel alloy [19] and AZ31 magnesium alloy [20]. The grain refinement from the machining process has improved surface integrity of the machined samples in terms of microstructure, microhardness, and residual stress [20,21]. Changes in the microstructure of any material can alter material properties such as hardness, strength, ductility, and corrosion resistance [2,22,23]. Microstructural changes generated by mechanical processing such as severe plastic deformation on the free surface of a workpiece are primarily characterized by the presence of deformed grains and grain refinement. Cutting parameters such as tool wear, cutting speed, feed rate and cooling affect the degree of plastic deformation [24]. Under aggressive cutting conditions, the high mechanical stress causes severe plastic deformation of the workpiece, resulting in a grain refinement layer on the machined surface layer. This grain refinement layer is also referred to as a “featureless layer” since there are no visible grain boundaries. In other words, the featureless layer is known as a white layer as it appears white after etching [25].

Coupled thermo-mechanical processes determine the thickness of white layers, which are affected by cutting parameters and material properties that determine mechanical stresses and cutting temperatures. Pu. et al. observed that the thickness of the white layer on AZ31 magnesium alloy increases with tool edge radius due to the increased deformation energy imposed on the machined surface [26]. Another study on machining AZ31 magnesium alloy revealed similar grain refinement under the machined surface [27]. The thickness of the white layer was 30 μm under dry cutting, while the cryogenic condition had a thickness of 20 μm . The reduction in white layer thickness following cryogenic turning was attributed to the additional impact of quenching caused by the flow of liquid nitrogen at the machining zone [28]. Dinesh et al. obtained comparable results while conducting cryogenic and dry-turning experiments on ZK60 magnesium alloy [13]. They observed that the featureless layer was created during cryogenic and dry turning operations on ZK60 magnesium alloy. However, the thickness of the featureless layer was decreased from 70 μm to 30 μm during cryogenic turning. The application of LN_2 reduces the grain size to nano size and limits grain growth, resulting in the formation of a featureless layer. A prior study found that the cryogenic machining of AZ31 magnesium alloy significantly influenced microhardness and microstructure [26]. The hardness beneath the machined surface was found to be the highest and gradually decreased to the nominal hardness when cutting AZ31 magnesium alloy [27]. The increase in microhardness was mainly

related to the effect of work hardening [13]. The cryogenic cooling, which was applied in cutting AZ31 magnesium alloy, produced the highest microhardness (97 Hv) compared to dry cutting, which recorded 86 Hv due to the hardening effect from the low temperature of cryogenic cooling [26]. Cryogenic cooling significantly enhanced grain refinement and surface integrity, resulting in better performance of machined components [26]. On the other hand, the microhardness of turned samples of AZ31 magnesium alloy under dry turning exhibited a declining trend with an increased cutting speed [21,27]. This situation was attributed to the dominance of the thermal softening effect which resulted from high temperature [29]. Machining of magnesium alloys often leads to a change in grain deformation near the machined surface [30,31].

Magnesium alloys have a distinct chip characteristic, with a lamellar structure that is visible on the free surface and a smooth surface at the tool-chip contact side [32]. Kuczmaszewski et al. conducted a study on milling AZ31 and AZ91HP magnesium alloy, and it was found that fragmented chips were obtained after the cutting process [3]. Saw-tooth and particle-type chips were observed during the turning of magnesium-based metal composites. The cutting speed was found to be the most significant factor that influenced the chip morphology and formation mechanism [33]. Pu et al. reported that serrated chips were formed in dry cutting and cryogenic cooling when turning AZ31 magnesium alloy. Adding a cooling element in the cutting zone was undeniably beneficial to the machinability of magnesium alloy [34,35]. In order to exploit the high specific heat capacity of water as heat absorbent in cutting magnesium alloy, internal cooling is a favorable approach as it avoids contact between water and magnesium. Bogajo et al. proposed an indirect cooling system whereby the cooling fluid flowed under the cutting zone [36]. The result of the study revealed a 12% improvement in surface roughness and a 12% reduction in cutting forces. Wu et al. designed a closed internal cooling tool by creating a cooling channel below the cutting insert, where water acted as a cooling fluid. The design successfully reduced the tool temperature by 60% [37]. Isik et al. conducted a turning experiment on nickel alloy using internally cooled cutting tools. A unique cooling channel was designed to remove heat from the cutting zone underneath the insert. The findings indicated a 12% increase in tool life and a 13% improvement in surface roughness [38]. Minton et al. investigated the effect of internal cooling tools on tool wear and life. Fabricating a fluid reservoir beneath the cutting insert has been found to reduce tool temperature and prevent it from exceeding the critical temperature. The study demonstrated that lower temperatures could suppress prominent wear mechanisms, resulting in a longer tool life [39]. Researchers have made significant advancements in designing an internal cooling system. However, there is still a lack of reported studies on chip morphology and surface integrity via internal cooling. The internal cooling approach, which involves cooling the top of the cutting insert, has not yet been revealed. Previously, the authors investigated the influence of cooling from SCC on the wear mechanism, cutting force, and temperature. The SCC successfully reduced built-up edge formation and cutting temperature [40]. Based on the aforementioned studies, it is evident that further studies are required to examine chip morphology and surface integrity of machined AZ31 magnesium alloy using an internal cooling approach.

Preventing the accumulation of heat at the cutting zone can improve the cutting performance of both the cutting insert and work material. In this paper, a turning experiment was conducted on AZ31 magnesium alloy using dry cutting and internal cooling. The internal cooling approach used in this study was known as submerged convective cooling (SCC). A novel approach to internal cooling was achieved by passively cooling the cutting insert with flowing cooled water on the top of the rake face, making the distance between the cooling and the cutting zone closer. The purpose of this work was to evaluate the efficacy of the SCC tool in enhancing cutting performance and expanding the use of SCC in the machining process. The chip morphology and surface integrity were examined in dry cutting and SCC to evaluate the cooling potency of internal cooling, specifically the SCC. The materials used in the turning experiment were described in Section 2. Section 3 mainly explained the chip morphology and surface integrity (microhardness, grain refinement,

and surface roughness) produced under dry cutting and SCC at different cutting speeds. Finally, Section 4 highlighted the findings and contributions of this study.

2. Materials and Methods

A CNC Turning T6 Compact Quicktech lathe was used in the turning experiment. The investigated material was the magnesium alloy AZ31 with a hardness of $55 \text{ Hv} \pm 1$. Its chemical compositions are listed in Table 1. The diameter and length of the workpiece were 30 mm and 100 mm, respectively.

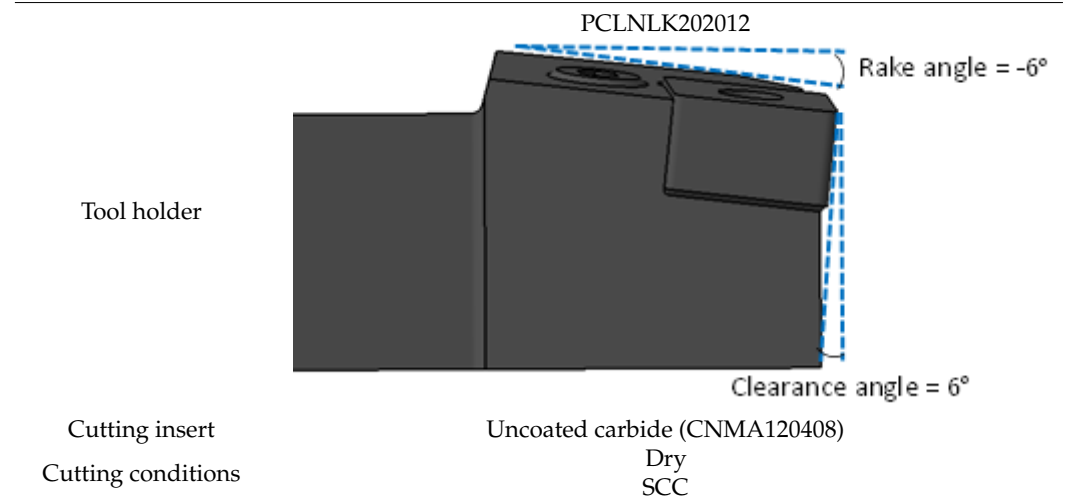
Table 1. Chemical composition of AZ31 magnesium alloy.

Chemical Composition (wt %)							
Material	Mg	Al	Zn	Mn	Si	Fe	Ca
AZ31	Bal	3.1	0.73	0.25	0.02	0.005	0.0014

All the machining conditions are shown in Table 2. The feed rate and depth of cut were held constant, while the cutting speed was varied to enhance heat generation. It was reported that the cutting temperature of AZ31 magnesium alloy was significantly impacted by the cutting speed [12]. The turning experiment was repeated three times for each cutting parameter and the measurement was taken at end stroke of cutting.

Table 2. Turning experimental conditions.

Cutting Parameters	Cutting speed (V_c)	120, 180, 240 m/min
	Depth of cut (a_p)	1 mm
	Feed rate (f)	0.2 mm/rev



The turning experiment was conducted in dry cutting and SCC. The cooling element was established at the cutting tool in the SCC cutting approach, which was achieved passively by allowing incoming cooling water to impinge on the tool rake face inside the cooling module to absorb heat from the cutting tool [41]. Figure 1 shows the components and circuit configuration of the SCC used in the current study proposed by Zakaria et al. [40]. The surface roughness was measured using Mitutoyo SJ-410 tester. The arithmetic average, R_a was measured per ISO 4287 standard with a 5 mm sampling length. R_a readings were taken at four different positions and an average was calculated. The chip morphology was analyzed using scanning electron microscopy (SEM) on a JEOL JSM-6010LV instrument. The microhardness of the samples was evaluated at the cross-section of the turned samples using Vickers' test with a load of 500 g and a dwell duration of 10 s on a Wolpert Wilson Microhardness Tester 402MVD. All microhardness measurements were

performed in accordance with ASTM E384. The microhardness of the sample was measured from just below the turned surface to the depth where the microhardness became constant. Every sample underwent three trials, and the average values were taken for analysis. For microstructure analysis of the turning samples, the concern surface was cut into a disk with a thickness of 10 mm. Grinding was performed using several SiC sandpapers with increasing grit sizes of 400, 600, 800, 1500, and 3000 in sequence at a speed of 150 rpm. Then, the samples were polished using MetaDi Supreme Crystalline Diamond Suspension with a particle size of 1 μm until the mirror image surface appeared at the concerned surface. The etchant used was an acetic picric solution, which is commonly preferred for etching magnesium alloys [21,26]. The acetic picric solution used in the study was freshly prepared by mixing 5 g of picric acid powder, 100 mL of ethanol, 10 mL of acetic acid, and 10 mL of water. After the samples were etched for a certain period, they were immersed in the acetic picric solution for 2 s and cleaned with ethanol. The samples were then dried using a blower and observed under the optical microscope Xoptron X80 series of high-power optical microscopy to study their microstructure.

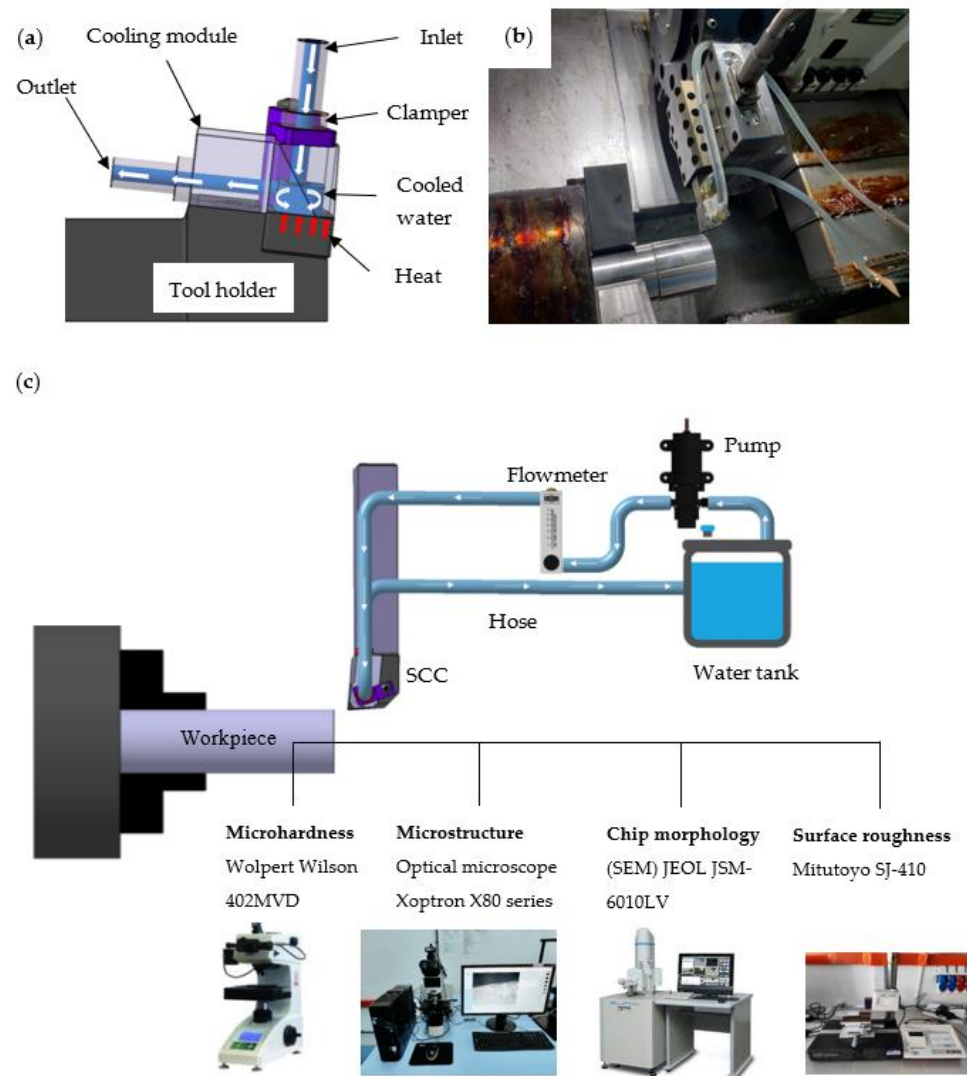


Figure 1. (a) SCC components [40] (b) SCC in CNC machine (c) experimental setup [40].

3. Results and Discussion

3.1. Chip Morphology

The present work analyzed chip morphology for each cutting speed in both conditions. A distinct chip type was observed in each condition. According to ISO3685 standards,

dry cutting produced ribbon-type chips, while SCC cutting produced arc-shaped chips. As shown in Figure 2, dry cutting produced continuous and tangled ribbon-type chips at both cutting speeds (120 and 180 m/min). At a higher cutting speed (240 m/min), the chips for dry cutting were continuous and long ribbon-type as shown in Figure 2. This was attributed to the improvement in material ductility as the temperature increased. A previous study reported that the temperature of AZ31 magnesium alloy increased as the cutting speed increased, leading to an increase in the elongation to fracture of the AZ31 [40]. This supported the improvement that was observed in the ductility [4]. The observed continuous chips in dry conditions could potentially occur due to the ductile nature of the magnesium alloy [26]. In SCC cutting, short and discontinuous chips (arc-connected type) were observed at all cutting speeds as shown in Figure 2. This type of chip could be due to lower cutting temperature in SCC, which restrained the temperature of the chip to increase and weakened the low intrinsic ductility of the material [42]. Furthermore, the alloy exhibited low strain-to-failure with decreasing temperature, which explained the shorter and discontinuous chip that was observed in SCC conditions [43]. In comparison to dry turning, the chips formed under SCC conditions were found to be shorter.

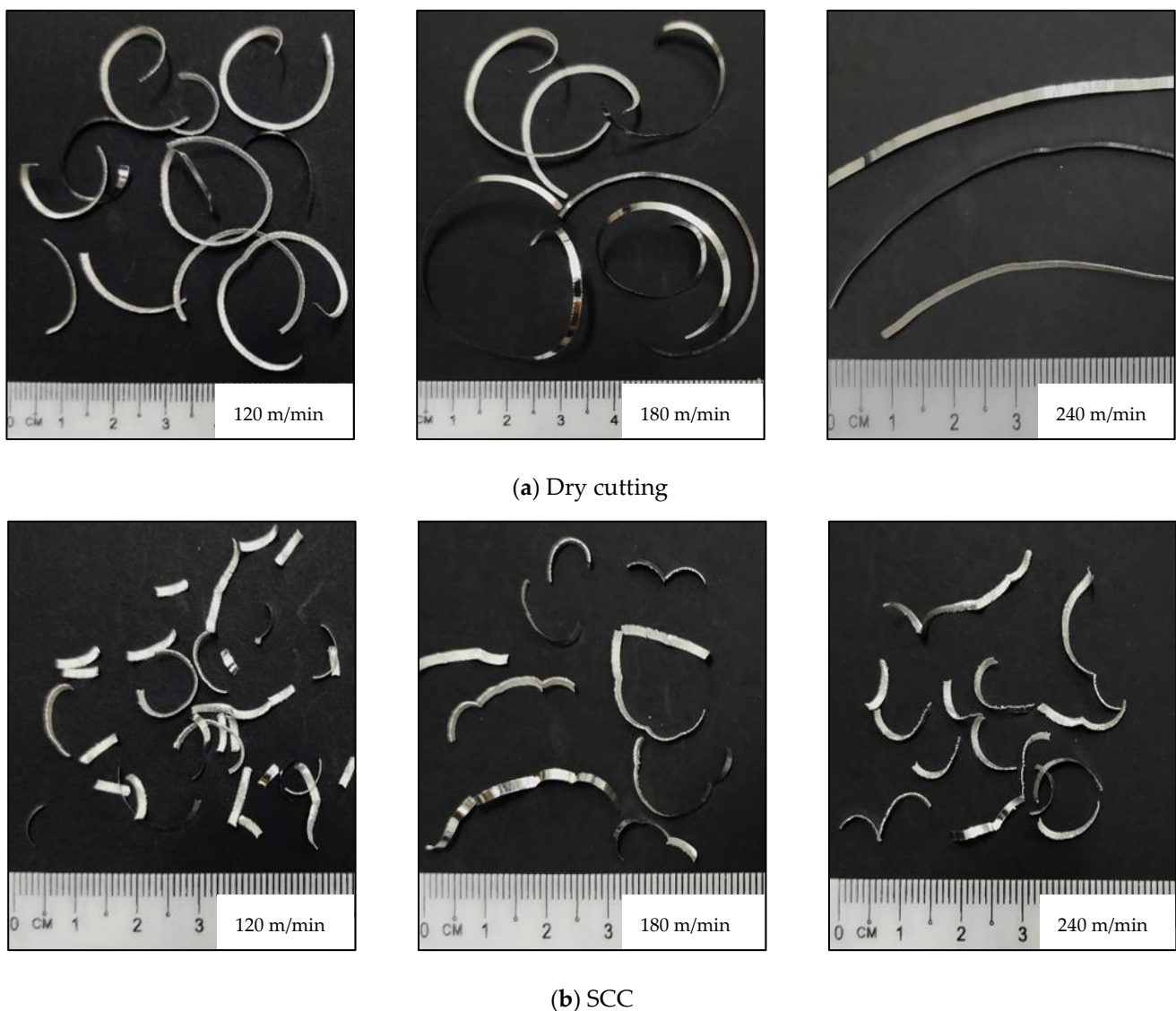


Figure 2. Effect of cutting speed and cutting conditions on the chip formation of AZ31 magnesium alloy.

In addition, the chips produced for all cutting speeds in dry cutting exhibited a higher curl compared to those produced in SCC, which were discontinuous and had a lower curl

as shown in Figure 2. This could be attributed to the cooling effect of the cutting fluid used in SCC [41]. In the machining process, smaller chip sizes are generally preferred, but these chips are prone to ignite. In the case of magnesium alloy, the risk of ignition increased as the chip size decreased [6]. Nevertheless, no sparks and chip ignitions were observed even at high cutting speeds in dry cutting, let alone in SCC condition, which had a cooling fluid that prevented an increase in temperature. The SEM images revealed that the produced chips had a serrated chip or saw-tooth shape, which was consistent with the findings of Pu [26] and was similar to the studies on machining AZ91D magnesium alloy [44]. Fundamentally, a serrated chip was formed when the crack initiated at the free surface and propagated toward the tooltip [45]. However, some reports argued that the formation of serrated chips is initiated at the tooltip and propagates to the free surface [46]. In this study, a serrated chip was observed on the free surface of the chip, while a smooth surface was observed on the back for all cutting speeds and cutting conditions. In addition, the presence of lamellas on the free surface of the chip indicated that adiabatic shear banding occurred throughout the cutting process. Based on the chips produced, the formation of serrated chips in dry cutting and SCC conditions could be attributed to high friction between the chip and tool as no lubrication was present in both cutting conditions. On the other hand, the chips produced in dry cutting were continuous and had almost no curling, implying that the material experienced severe ductility at a high strain rate and high temperature. According to Feng et al. and Zhang et al., AZ31 magnesium alloy demonstrated high strain at a high strain rate and temperature due to its softening behavior [47,48]. Reducing the temperature of AZ31 magnesium alloy while maintaining the same strain rate caused the material to lose ductility, resulting in a lower strain value [49]. Therefore, at the same cutting speed, the lower cutting temperature in SCC produced short and discontinuous chips due to the curling effect and low ductility of the work material as shown in Figure 2. It was reported that the brittleness of the magnesium alloy increased with decreasing temperature, thus aiding in chip breakability [50].

The chip back surface revealed the condition of material adhesion at the tool-chip interface, affecting the surface produced on the work material [51]. As shown in Figure 3, material adhesion was seen at the chip-back surface in dry cutting, while a smoother chip-back surface with less material adhesion was depicted in SCC. This observation suggests that material adhesion at the cutting tool was carried away from the flowing chip, resulting in high shear force. When the cutting speed was increased to 180 m/min, the chip-back surface was marginally improved, with material adhesion and particle still present in the dry cutting. This was attributed to the high chip velocity and strain rate, which produced enormous heat and caused the work material to melt instead of completely adhering to the tool. However, the cooling effect in SCC prevented the temperature of the work material from exceeding the melting temperature, resulting in less material adhesion and a smooth back surface of the chip. The chip curl was larger than the chip at the cutting speed of $V = 120$ m/min. The ductility of AZ31 magnesium alloy increased with elevated temperature; therefore, a larger chip curl was obtained as the cutting speed increased [52]. Less material adhesion was observed on the back surface of the chip at $V = 240$ m/min, with adhesion only in the form of particles in dry cutting and almost no particle adhesion for SCC condition. This was mainly attributed to intense heat generation at high cutting speed ($V = 240$ m/min) coupled with high chip velocity, resulting in less contact time between the chip and tool that would cause material adhesion. On the back surface of the chips, cracks were observed to occur and propagate in opposite directions. The primary cause of these cracks is the strong friction between rake faces and chips as there was no presence of lubrication.

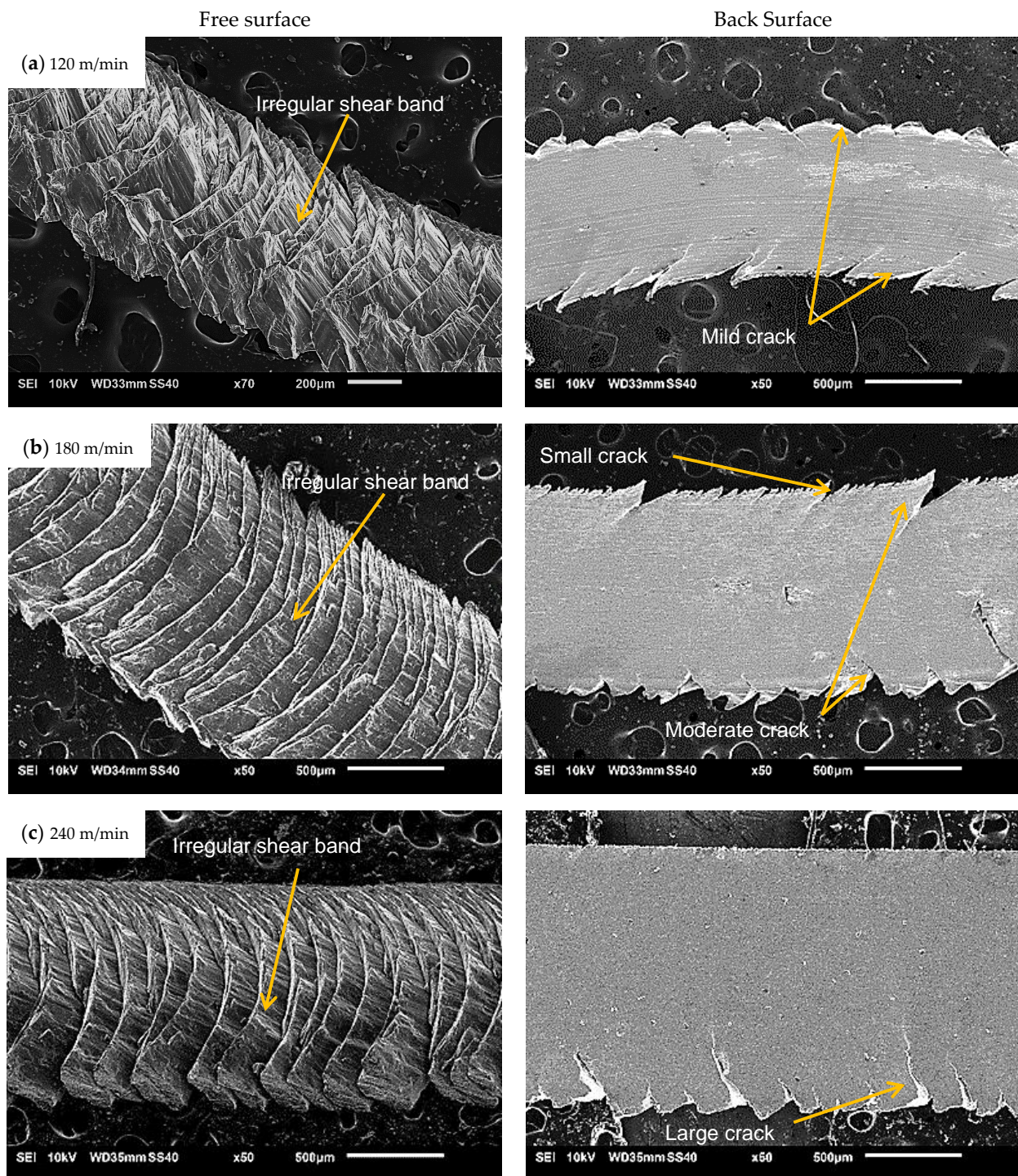


Figure 3. Chip morphology of front surface and back surface for dry cutting.

In dry cutting, mild cracks were observed in both edges at a cutting speed of 120 m/min speed, propagating to the center of the chip. When the cutting speed was increased to 180 m/min, a combination of cracks was observed on one side, while moderate cracks remained regular on the opposite side. At a high cutting speed of $V = 240$ m/min, cracks were almost unnoticeable on one side and fewer large cracks were observed on the opposite side. These cracks were consistent with the chip produced in dry cutting at respective cutting speeds as the cracks aided in chip breakability at low cutting speeds. However, it evolved to a long ribbon continuous chip at high cutting speed. This phenomenon could

be attributed to the ductile characteristics of the material, which improved with increasing temperature and strain rate [53]. The ductile character of the produced chip was shown by the rapid halt of fracture propagation which was caused by the closure of the ductile magnesium ahead of the crack [54]. Furthermore, cracks were seen at the back surface of the chips for the SCC cutting condition. At low cutting speed of $V = 120$ m/min, mild and severe cracks occurred at the back surface of the chip. These cracks facilitated the ease of chip breaking to produce the discontinuous chip. Increasing the cutting speed to 180 m/min caused the material to experience intense plastic deformation, leading to large cracks on both chip edges. As the cutting speed increased, the temperature and strain rate also increased. This caused severe cracks on the back surface of the chip at the cutting speed of $V = 240$ m/min, indicating that the intensity of plastic deformation and friction. In SCC, the cooling effect prevented thermal softening from surpassing the strain hardening effect, causing the work material to fail in a brittle manner instead of having a ductile failure [53] to produce a discontinuous chip. The severity of chip cracks was even more pronounced in SCC with an increased cutting speed as shown in Figure 4, with considerable deep crack propagation and brittle behavior resulting from cooling in SCC. When comparing the chip-free surface between dry cutting and SCC, similar shear band patterns were observed in both cutting conditions as shown in Figures 3 and 4, resulting in shear instability. Liyao et al. reported that adiabatic shear instability and catastrophic strain localization were the primary causes of segmented chip formation [55]. The shear band became denser, indicating an increased cutting speed due to more intense plastic deformation and a higher thermal softening effect [56]. The compactness of shear bands at the free surface of the chip was slightly reduced for respective cutting speeds due to the cooling effect in SCC. This was mainly attributed to the lower thermal softening effect that was achieved in SCC.

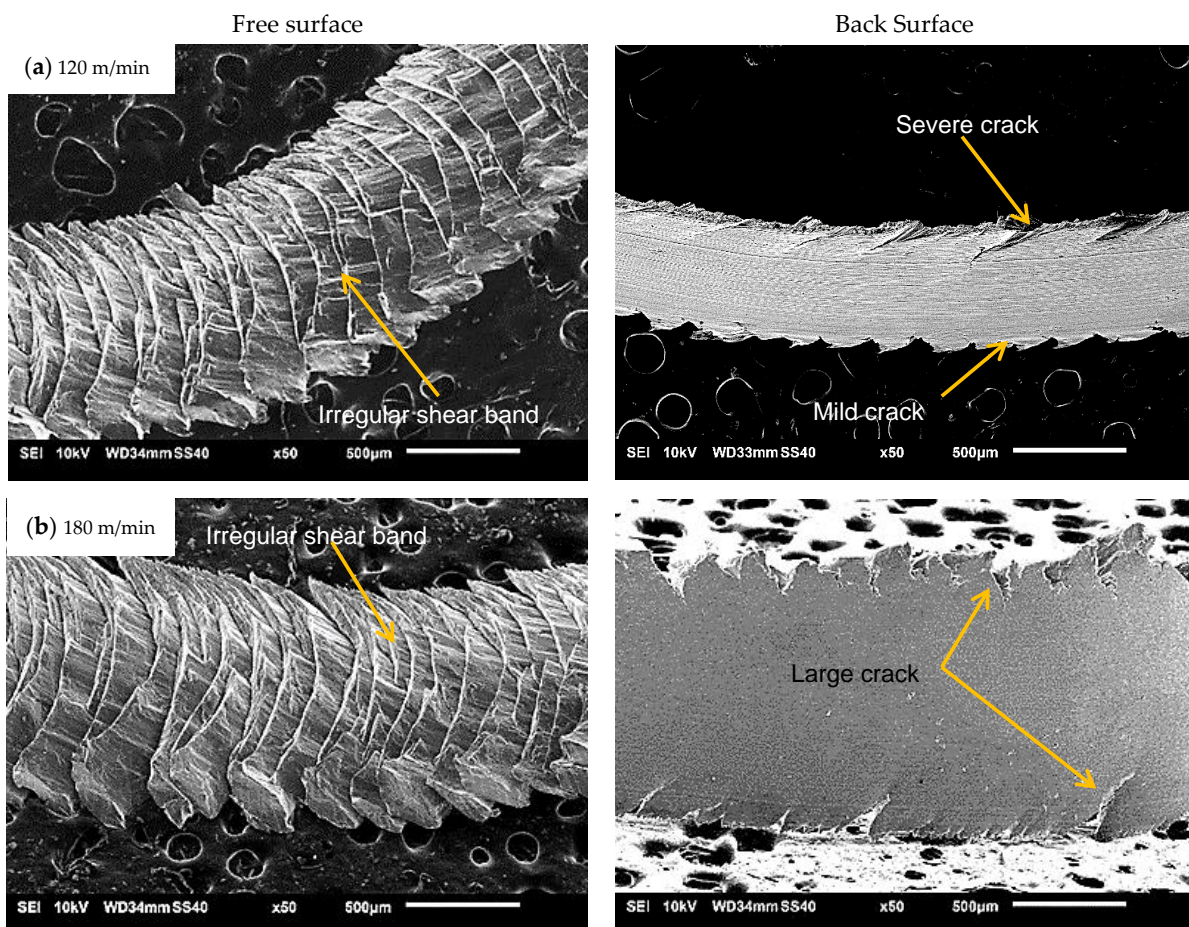


Figure 4. Cont.

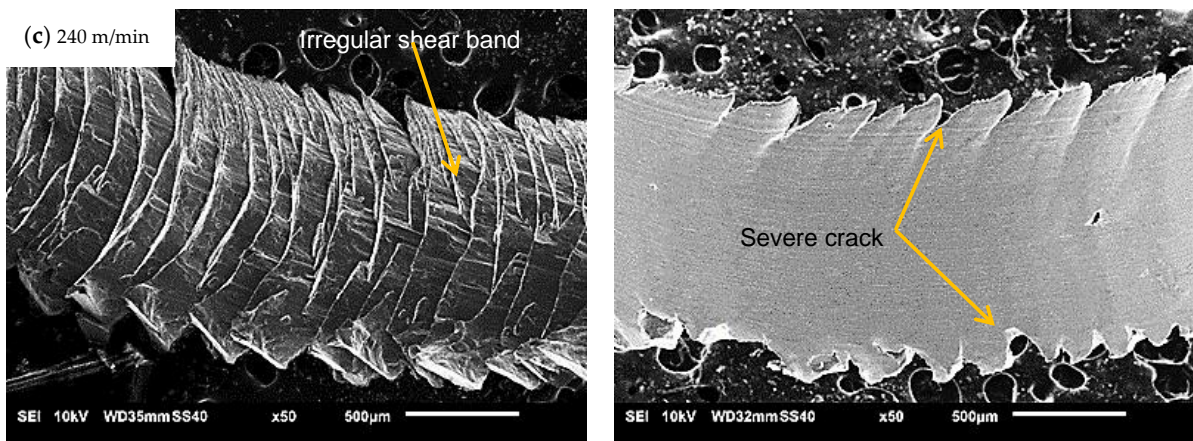


Figure 4. Chip morphology of front surface and back surface for SCC cutting.

3.2. Microstructure

This section provided a microstructural analysis that was conducted on the machined sample at different cutting speeds to elucidate the effect of cooling from SCC and dry cutting. The microstructure of AZ31 magnesium alloy before the cutting process at the cross-section of the as-received sample is shown in Figure 5. The grain boundaries were visible, and dynamic recrystallization grains were spotted at the cross-sectional area. Some coarse grains had a size of up to 115 micrometers, while the smallest grains had a size of 7 μm . The statistically significant grain size was determined to be between 20 μm to 100 μm . Figure 5b depicts grain boundaries at the edge of the sample. The grain boundaries were intact and had almost similar sizes as those in the middle of the sample in Figure 5a. The grains had predominantly irregular shapes with the presence of a few dendritic grains, which was consistent with previous studies that used the same series of magnesium alloy [57–59].

Figures 6 and 7 showed that a “featureless layer” was formed where grain boundaries were no longer visible under the magnification used at higher cutting speeds in both dry and SCC conditions. The grain size in the featureless layer was reported to have achieved nanocrystalline grains when examined using atomic force microscopy (AFM), which revealed ultrafine grains ranging from 30 nm to 60 nm in size [20].

Thermal softening is induced by increasing cutting speed due to plastic deformation and friction. This led to an increase in temperature, which affected the machined surface and subsurface. The grain refinement was initiated by dynamic recrystallization (DRX) with an increased cutting speed [26]. The appearance of the featureless layer in dry cutting was similar to a previous study on turning the same series of magnesium alloy [21,26]. The “featureless layer” was also referred to as the residual stress layer, which originated from severe plastic deformation under the action of cutting force where the work hardening effect remained in the machined surface [20]. This layer was also referred to as the heat-affected zone (HAZ) [13]. An empirical equation proposed by Watanabe et al. predicted that the recrystallized grains were distinctly related to the temperature factor for grain refinement as shown in Equations (1) and (2) [60].

$$\frac{d_{rec}}{d_{init}} = 10^3 \cdot Z^{\frac{1}{3}} \quad (1)$$

where d_{rec} is recrystallized grain size, d_{init} is the initial grain size, and Z is the Zener–Holloman parameter which was defined as follows:

$$Z = \dot{\epsilon} e^{\left(\frac{Q}{RT}\right)} \quad (2)$$

where $\dot{\epsilon}$ is the strain rate, Q is the activation energy, R is the gas constant, and T is the temperature. From Equation (2), it was deduced that Z was inversely proportional to the temperature. As the temperature increased, the value of Z decreased, resulting in a smaller grain size, which was not visible under the optical microscope used in this study. Both dry and SCC conditions depicted an increasing temperature with cutting speed, which was also reported by Danish et al. [12]. When comparing the microstructure of dry and SCC conditions, the thickness of the featureless layer in dry turning was thicker than that in SCC at all cutting speeds. For a cutting speed of 120 m/min, the featureless layer had a thickness of 7 μm for dry cutting, while the featureless layer for SCC showed a thickness of 5.5 μm . The featureless layer was further increased to 10 μm and 9 μm when the cutting speed increased to 180 m/min in dry cutting and SCC, respectively. When the cutting speed was increased to 240 m/min, the thickness of the featureless layer increased to 12 μm in dry cutting, while the thickness of the layer was 10 μm in SCC. The observed pattern of the thickness of the featureless layer between dry cutting and SCC inferred that the cooling provided by SCC at the cutting zone was effective in restricting the propagation of HAZ thickness. This pattern was also reported in cryogenic turning, whereby the thickness of the featureless layer decreased for cryogenic turning samples due to the cooling effect [13,61]. Furthermore, the dominance of BUE and BUL formation in dry cutting led to a deeper featureless layer compared to SCC [40]. The alteration of the edge radius due to BUE and BUL formation led to a large edge radius, which caused a greater burnishing effect on the work material at greater depths. This was in line with the study conducted by Pu, in which a larger edge radius changed the microstructure at greater depths [26].

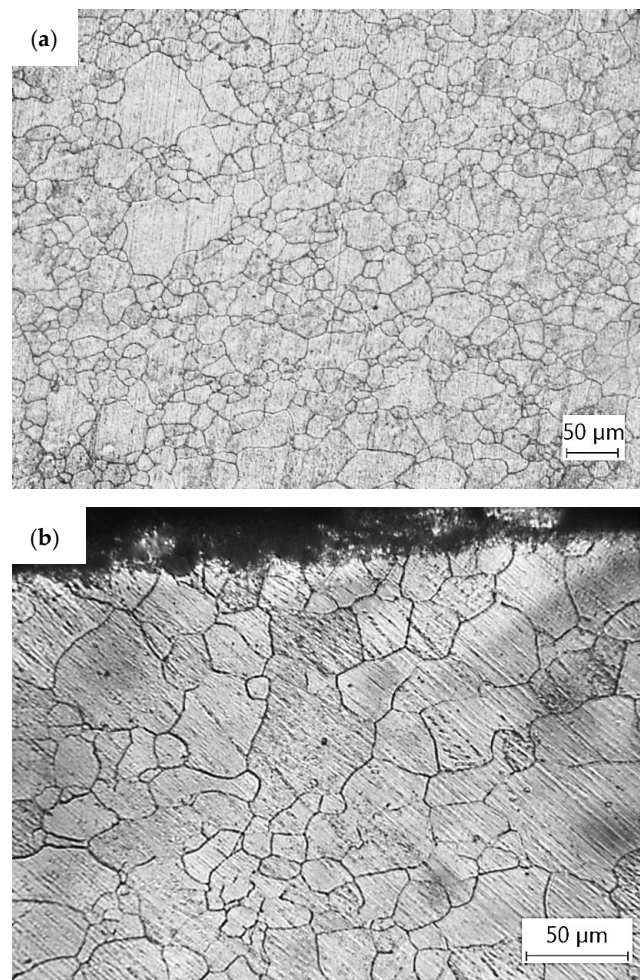


Figure 5. Microstructure of AZ31 magnesium alloy before turning process (a) in the middle (b) close to the edge.

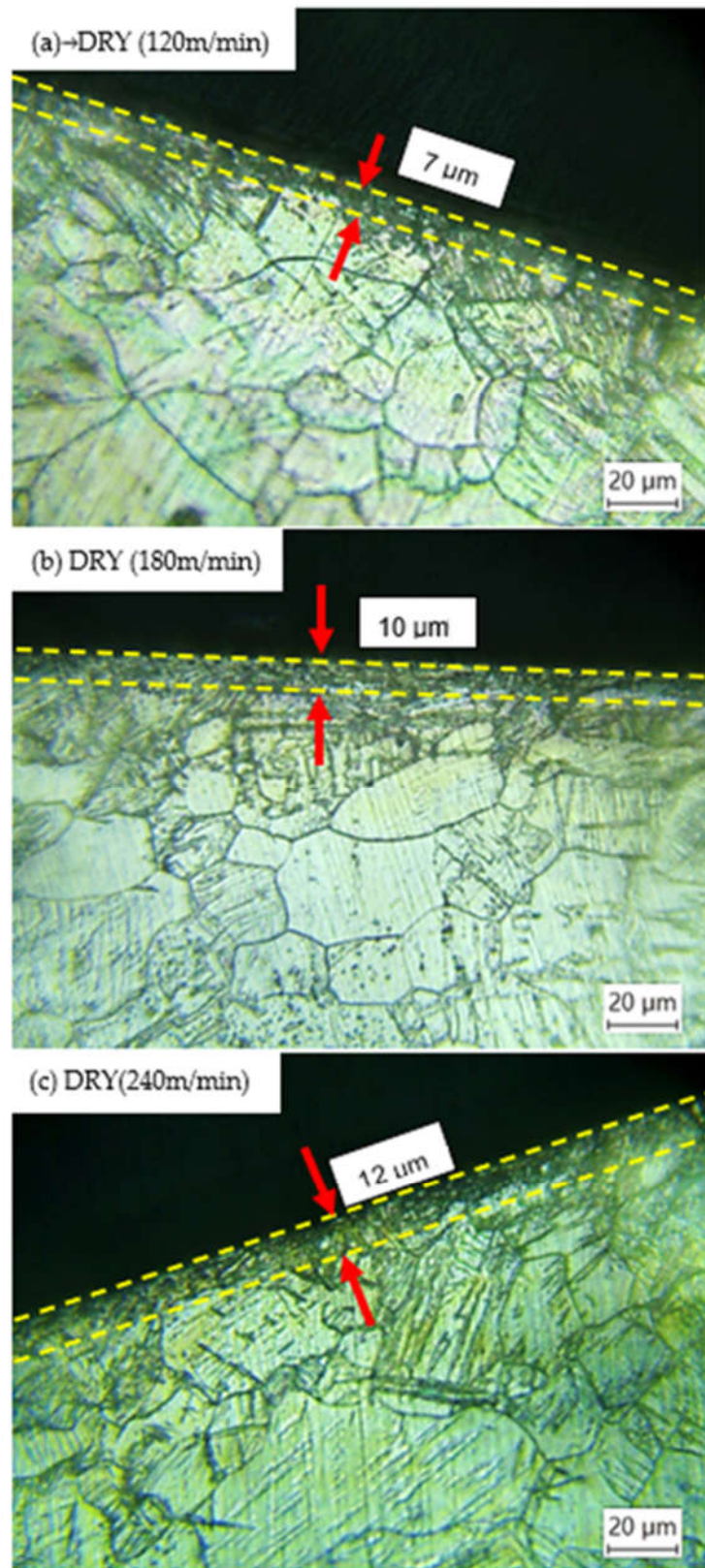


Figure 6. Microstructure of machined surface under dry condition.

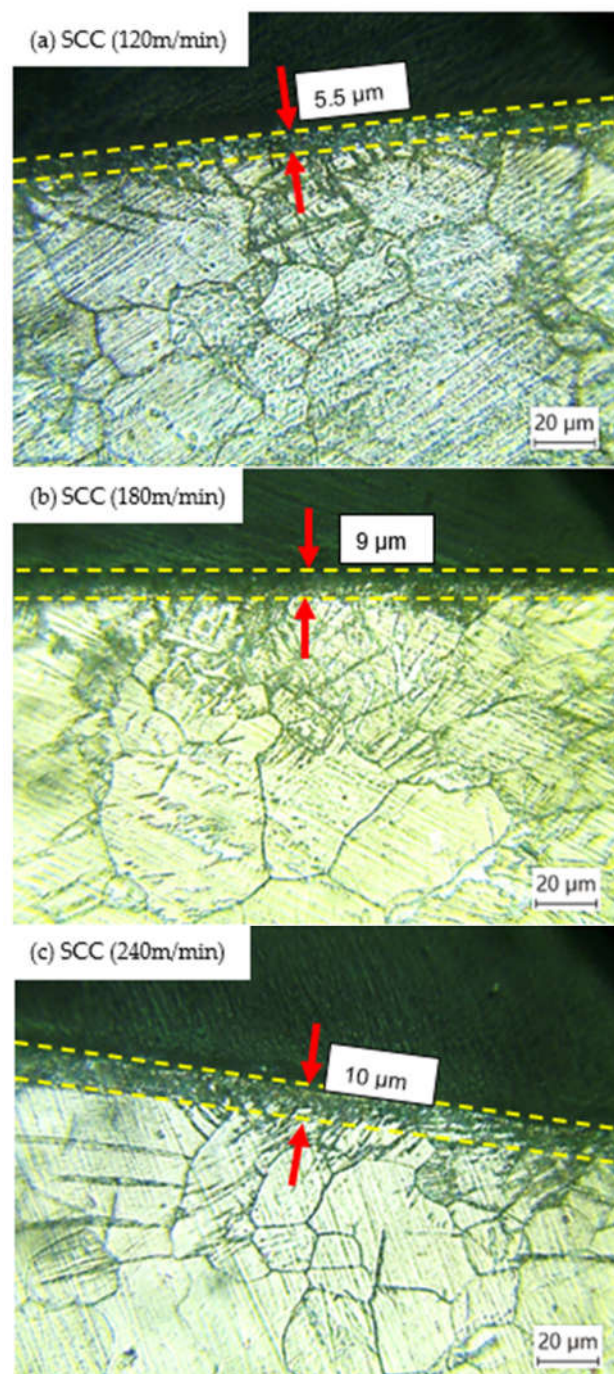


Figure 7. Microstructure of the machined surface under SCC condition.

3.3. Microhardness

This section explained the effect of the SCC condition on the hardness variation. In order to evaluate the hardness of AZ31 magnesium alloy, the hardness of received, dry, and SCC-turned samples were measured and compared. Figure 8 shows the hardness of AZ31 magnesium alloy as a function of depth from the machined surface at a cutting speed of 120 m/min. The average hardness of AZ31 magnesium alloy was 55 Hv. The results indicated that the highest hardness values were observed near the machined surface (0.05 mm below the machined surface) for dry cutting and SCC. The microhardness is directly related to the grain size [61]. The findings were consistent with the previous study conducted by Srinivasan et al., who found that packed grains with small dimensions have

a higher microhardness value [62]. As shown in Figure 9, the highest hardness value was observed at a cutting speed of $V = 120$ m/min in SCC with an increase of 60.5% from 55 Hv to 88.3 Hv. On the other hand, dry cutting only resulted in a 49% increase in the hardness of 82 Hv. Dominating strain hardening due to the plastic deformation process in turning AZ91 was responsible for increasing compressive yield strength, which exhibited a small grain size compared to the as-received material [63]. As the cutting speed increased to 180 m/min, the hardness of the machined sample under SCC and dry cutting reduced to 82.5 Hv and 77.2 Hv, respectively. Dry cutting recorded the lowest hardness at a cutting speed of $V = 240$ m/min, where the hardness value was 73.2 Hv and 75.9 Hv for the SCC-turned sample. The deviation in microhardness of turned samples between SCC and dry cutting could be due to the fact that the hardening degree of machined samples depends on plastic deformation and heat intensity [21]. During the cutting process, severe plastic deformation leads to material hardening behavior, while tremendous heat generation causes thermal softening at the machined surface. Increasing the cutting speed always induces enormous heat generation which resulted from work material deformation and enhances the thermal softening effect, thus reducing surface hardening with increased cutting speed.

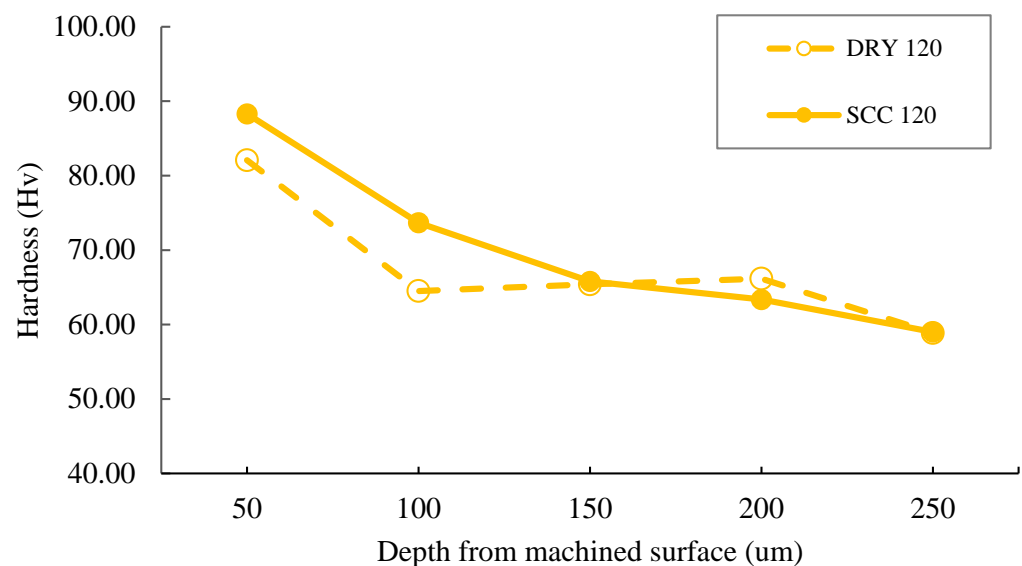


Figure 8. AZ31 magnesium alloy microhardness as a function of depth from the turned surface for dry cutting and SCC-turned samples ($V = 120$ m/min).

A similar trend was observed in dry cutting, whereby the hardness of the machined surface decreased with the cutting speed. When comparing dry cutting to the SCC condition, the hardness of AZ31 magnesium alloy below the machined surface produced a higher hardness in the SCC condition for all cutting speeds. This was in agreement with the findings of Pu in cryogenic turning, in which the hardness of AZ31 magnesium alloy outperformed dry turning due to grain refinement [26]. Danish et al. reported that dominant dynamic recrystallization, which was because of low temperature in cryogenic cutting, resulted in high microhardness of AZ31-turned samples over dry turning [64]. Cooled tools under SCC conditions undermined the thermal softening effect and work hardening dominance at the machined surface, increasing the hardness of the SCC machined samples. Danish et al. investigated a turning experiment on Inconel 718 with different lubrication and cooling conditions. The study revealed that when in cryogenic + MQL conditions, the samples produced the highest microhardness on the machined surface due to the rapid cooling effect [19]. Based on BUE formation in SCC cutting, less material adhesion at the cutting tool tended to reduce the temperature in the cutting zone with cooling provided by the cutting tool [40]. Less material adhesion reduced thermal resistance for heat exchange between the machined surface and cutting tool. Therefore, the cooled flank surface of

the cutting tool, which had direct contact with the machined surface, could absorb the generated heat and subsequently suppress the thermal softening.

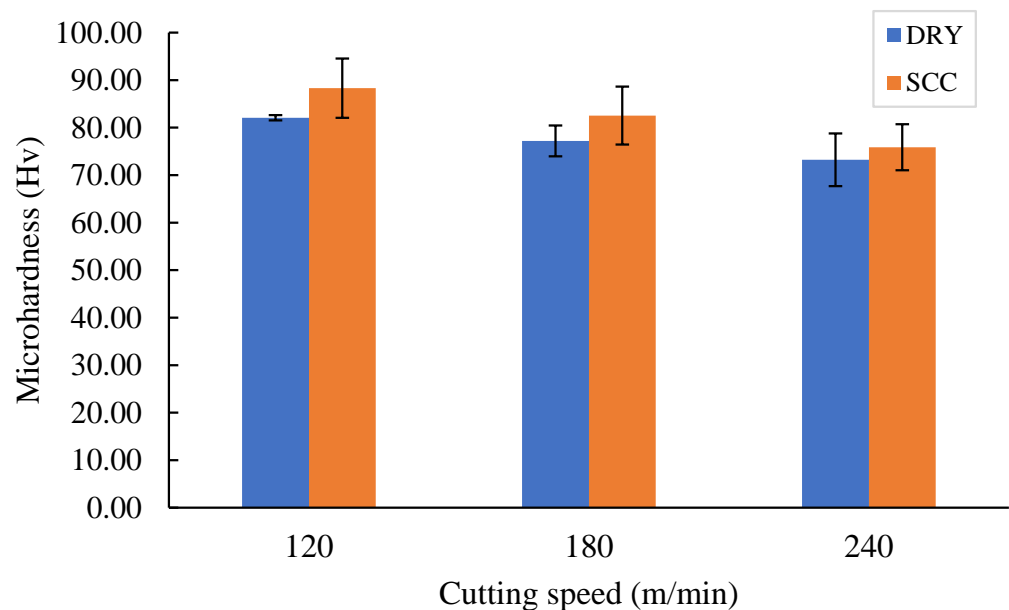


Figure 9. Microhardness at 0.05 mm below the surface of dry and SCC-turned samples.

3.4. Surface Roughness

Surface roughness due to the machining process is a crucial factor in the corrosion resistance of AZ31 magnesium alloy as well as part accuracy for assembly purposes and tribological behavior [65]. It was observed that cutting speed greatly influenced surface roughness when machining AZ31 magnesium alloy [21]. Figure 10 shows the average surface roughness under different drying and SCC cutting speeds. The surface roughness was lowered with an increased cutting speed in both cutting conditions, which was in line with the reported literature [12]. Increased cutting speed stimulated softening of the material as the cutting temperature increased, which minimized tool chatter. Yousefi et al. explained that this phenomenon could be the reason for improved surface roughness [66]. SCC surpassed dry cutting at all cutting speeds. The lowest surface roughness ($R_a = 1.564 \mu\text{m}$) was measured on the workpiece at a cutting speed of 240 m/min, while the highest surface roughness of $1.903 \mu\text{m}$ was achieved in dry cutting for at a cutting speed of 120 m/min. SCC reduced the R_a values by 10.8%, 9.4% and 4.7% for cutting speeds of 120, 180, and 240 m/min, respectively, when compared to dry cutting. Both cutting conditions exhibited improved surface roughness as the cutting speed increased. This was mainly attributed to increased heat generation at high cutting speed. This led to a decrease in BUE and BUL formation as the cutting speed increased, resulting in better surface roughness [40]. Despite the absence of lubrication in SCC, the cooling effect in the SCC had a positive impact on surface quality. This result was in line with the previous study, which claimed that cooling from cryogenic liquid nitrogen significantly reduced the surface roughness of AZ31 magnesium alloy [26]. The cooling effect in SCC contributed to a lower cutting temperature and reduced material adhesions at the cutting tool, resulting in a smooth surface roughness that was similar to that of cryogenic cutting [19,67].

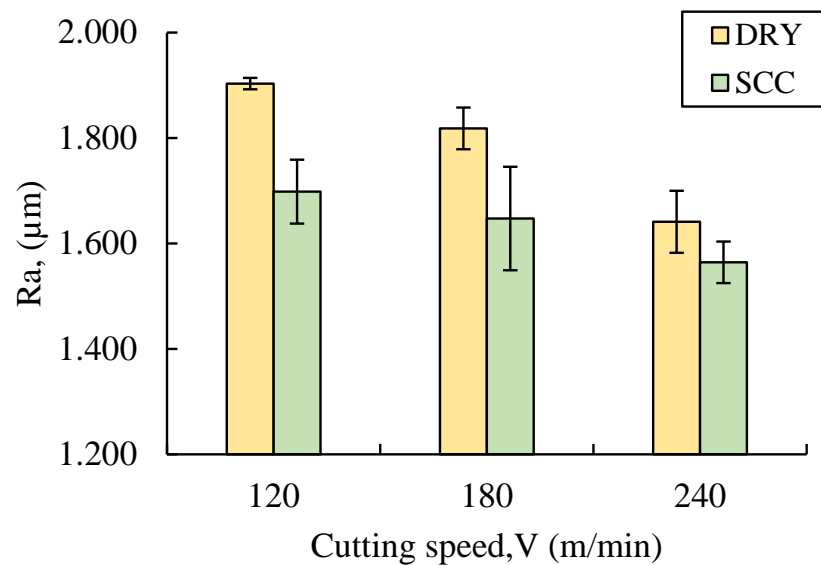


Figure 10. Effect of cutting speed for dry cutting and SCC on surface roughness.

4. Conclusions

This study presented the application of SCC in turning AZ31 magnesium alloy compared to conventional dry cutting. The study proposed an internal cooling approach in SCC, which involved passive cooling on the top of the cutting insert to reduce the distance between the cooling and heat source. The potential of the SCC tool was investigated by varying the cutting speeds to generate significant heat for analyzing chip morphology and surface integrity analysis during the cutting process.

- SCC and dry cutting produced chips with saw-tooth shapes for all cutting speeds.
- Continuous and ribbon-type chips were observed in dry cutting due to improvement in the ductility of work material.
- The cooling effect in SCC had a significant impact on the chip formation, leading to the presence of discontinuous and arc-shaped chips because of the increased brittleness of AZ31 magnesium alloy that was caused by a decrease in temperature.
- SEM images revealed a severe crack at the back surface of the chip in SCC, which occurred because of the brittleness of AZ31 magnesium alloy that was resulted from the cooling effect in SCC.
- The work-hardening effect induced by the cooling effect in SCC has played a significant role in reducing thermal softening. This resulted in a thinner featureless layer beneath the machined surface as it restrained the propagation of HAZ thickness.
- The use of SCC resulted in higher microhardness values for the respective cutting speeds compared to dry cutting due to the dominance of work hardening at the machined sample. The SCC increased the hardness of the AZ31-turned sample by 60.5%, while dry cutting only resulted in an increase of 49% in microhardness.
- Due to the cooling effect in SCC, less material adhesion occurred at the back surface of the chip, resulting in better surface roughness compared to dry cutting. SCC achieved a 10.8%, 9.4%, and 4.7% improvement in surface roughness for cutting speeds of 120, 180, and 240 m/min, respectively, compared to dry cutting.

Author Contributions: Conceptualization, M.S.Z.; methodology, A.I.A.; software, C.Y.K.; validation, M.S.Z.; formal analysis, M.M.; investigation, C.Y.K.; resources, M.M.; data curation, M.S.Z.; writing—original draft preparation, M.S.Z.; writing—review and editing, C.Y.K.; visualization, C.Y.K.; supervision, M.M. and A.I.A.; project administration, C.Y.K.; funding acquisition, M.S.Z. and A.I.A.; All authors have read and agreed to the published version of the manuscript.

Funding: This work was supported by the Ministry of Higher Education, Malaysia under the grant number FRGS/1/2020/TK0/UNIMAP/03/15.

Data Availability Statement: The data presented in this study are available on request from the corresponding author.

Acknowledgments: We are very grateful to the Ministry of Higher Education, Malaysia for providing financial support under the Fundamental Research Grant Scheme (FRGS) with the grant number FRGS/1/2020/TK0/UNIMAP/03/15.

Conflicts of Interest: The authors declare no conflict of interest.

References

1. Salvetr, P.; Novák, P.; Vojtěch, D. Magnesium Alloys for Implants. *Manuf. Technol.* **2013**, *13*, 395–399. [[CrossRef](#)]
2. Chen, J.; Tan, L.; Yu, X.; Etim, I.P.; Ibrahim, M.; Yang, K. Mechanical Properties of Magnesium Alloys for Medical Application: A Review. *J. Mech. Behav. Biomed. Mater.* **2018**, *87*, 68–79. [[CrossRef](#)] [[PubMed](#)]
3. Zagórski, I.; Kuczmaszewski, J. Temperature Measurements in the Cutting Zone, Mass, Chip Fragmentation and Analysis of Chip Metallography Images during AZ31 and AZ91HP Magnesium Alloy Milling. *Aircr. Eng. Aerosp. Technol.* **2018**, *90*, 496–505. [[CrossRef](#)]
4. Dieringa, H. Influence of Cryogenic Temperatures on the Microstructure and Mechanical Properties of Magnesium Alloys: A Review. *Metals* **2017**, *7*, 38. [[CrossRef](#)]
5. Fang, F.Z.; Lee, L.C.; Liu, X.D. Mean Flank Temperature Measurement in High Speed Dry Cutting of Magnesium Alloy. *J. Mater. Process. Technol.* **2005**, *167*, 119–123. [[CrossRef](#)]
6. Carou, D.; Rubio, E.M.; Lauro, C.H.; Davim, J.P. Experimental Investigation on Surface Finish during Intermittent Turning of UNS M11917 Magnesium Alloy under Dry and near Dry Machining Conditions. *Measurement* **2014**, *56*, 136–154. [[CrossRef](#)]
7. Berzosa, F.; De Agustina, B.; Rubio, E.M. Tool Selection in Drilling of Magnesium UNSM11917 Pieces under Dry and MQL Conditions Based on Surface Roughness. *Procedia Eng.* **2017**, *184*, 117–127. [[CrossRef](#)]
8. Zhang, H.; Zhao, P.; Ge, Y.; Tang, H.; Shi, Y. Chip Morphology and Combustion Phenomenon of Magnesium Alloys at High-Speed Milling. *Int. J. Adv. Manuf. Technol.* **2018**, *95*, 3943–3952. [[CrossRef](#)]
9. Yu, A.; Wang, S.; Li, N.; Hu, H. Pressurized Solidification of Magnesium Alloy AM50A. *J. Mater. Process. Technol.* **2007**, *191*, 247–250. [[CrossRef](#)]
10. Blanco, D.; Rubio, E.M.; Sáenz-Nuño, M.A.; Lorente-Pedreille, R.M. Comparison of Sustainable Cooling Systems Used in the Drilling Repair of Mg-Al and Mg-Ti Multi-Material Parts in the Aeronautical Industry. *Tribol. Int.* **2022**, *175*, 107804. [[CrossRef](#)]
11. Khanna, N.; Shah, P.; Suri, N.M.; Agrawal, C.; Khatkar, S.K.; Pusavec, F.; Sarikaya, M. Application of Environmentally-Friendly Cooling/Lubrication Strategies for Turning Magnesium/SiC MMCs. *Silicon* **2020**, *13*, 2445–2459. [[CrossRef](#)]
12. Danish, M.; Ginta, T.L.; Habib, K.; Carou, D.; Rani, A.M.A.; Saha, B.B. Thermal Analysis during Turning of AZ31 Magnesium Alloy under Dry and Cryogenic Conditions. *Int. J. Adv. Manuf. Technol.* **2017**, *91*, 2855–2868. [[CrossRef](#)]
13. Dinesh, S.; Senthilkumar, V.; Asokan, P.; Arulkirubakaran, D. Effect of Cryogenic Cooling on Machinability and Surface Quality of Bio-Degradable ZK60 Mg Alloy. *Mater. Des.* **2015**, *87*, 1030–1036. [[CrossRef](#)]
14. Danish, M.; Ginta, T.L.; Wahjoedi, B.A. Enhanced Functional Properties of Mg Alloys by Cryogenic Machining. *Int. J. Appl. Eng. Res.* **2016**, *11*, 5055–5059.
15. Dinesh, S.; Senthilkumar, V.; Asokan, P. Experimental Studies on the Cryogenic Machining of Biodegradable ZK60 Mg Alloy Using Micro-Textured Tools. Predictive Modelling and M. *Manuf. Process.* **2017**, *32*, 979–987. [[CrossRef](#)]
16. Eker, B.; Ekici, B.; Kurt, M.; Bakýr, B. Sustainable Machining of the Magnesium Alloy Materials in the CNC Lathe Machine and Optimization of the Cutting Conditions. *Mechanics* **2014**, *20*, 310–316. [[CrossRef](#)]
17. Gziut, O.; Kuczmaszewski, J.; Zagórski, I. Surface quality assessment following high performance cutting of AZ91HP magnesium alloy. *Manag. Prod. Eng. Rev.* **2015**, *6*, 4–9. [[CrossRef](#)]
18. Gao, H.; Ma, B.; Singh, R.P.; Yang, H. Areal Surface Roughness of AZ31B Magnesium Alloy Processed by Dry Face Turning: An Experimental Framework Combined with Regression Analysis. *Materials* **2020**, *13*, 2303. [[CrossRef](#)]
19. Danish, M.; Gupta, M.K.; Rubaiee, S.; Ahmed, A.; Korkmaz, M.E. Influence of Hybrid Cryo-MQL Lubri-Cooling Strategy on the Machining and Tribological Characteristics of Inconel 718. *Tribol. Int.* **2021**, *163*, 107178. [[CrossRef](#)]
20. Shen, N.; Ding, H.; Pu, Z.; Jawahir, I.S.; Jia, T. Enhanced Surface Integrity from Cryogenic Machining of AZ31B Mg Alloy: A Physics-Based Analysis with Microstructure Prediction. *J. Manuf. Sci. Eng. Trans. ASME* **2017**, *139*, 061012. [[CrossRef](#)]
21. Lu, L.; Hu, S.; Liu, L.; Yin, Z. High Speed Cutting of AZ31 Magnesium Alloy. *J. Magnes. Alloy.* **2016**, *4*, 128–134. [[CrossRef](#)]
22. Agarwal, S.; Curtin, J.; Duffy, B.; Jaiswal, S. Biodegradable Magnesium Alloys for Orthopaedic Applications: A Review on Corrosion, Biocompatibility and Surface Modifications. *Mater. Sci. Eng. C* **2016**, *68*, 948–963. [[CrossRef](#)] [[PubMed](#)]
23. Wang, Q.; Liu, Z.; Wang, B.; Song, Q.; Wan, Y. Evolutions of Grain Size and Micro-Hardness during Chip Formation and Machined Surface Generation for Ti-6Al-4V in High-Speed Machining. *Int. J. Adv. Manuf. Technol.* **2016**, *82*, 1725–1736. [[CrossRef](#)]
24. Wojciechowski, S.; Matuszak, M.; Powalka, B.; Madajewski, M.; Maruda, R.W.; Królczyk, G.M. Prediction of Cutting Forces during Micro End Milling Considering Chip Thickness Accumulation. *Int. J. Mach. Tools Manuf.* **2019**, *147*, 103466. [[CrossRef](#)]

25. Liao, Z.; la Monaca, A.; Murray, J.; Speidel, A.; Ushmaev, D.; Clare, A.; Axinte, D.; M'Saoubi, R. Surface Integrity in Metal Machining—Part I: Fundamentals of Surface Characteristics and Formation Mechanisms. *Int. J. Mach. Tools Manuf.* **2021**, *162*, 103687. [[CrossRef](#)]
26. Pu, Z.; Outeiro, J.C.; Batista, A.C.; Dillon, O.W.; Puleo, D.A.; Jawahir, I.S. Enhanced Surface Integrity of AZ31B Mg Alloy by Cryogenic Machining towards Improved Functional Performance of Machined Components. *Int. J. Mach. Tools Manuf.* **2012**, *56*, 17–27. [[CrossRef](#)]
27. Danish, M.; Ginta, T.L.; Rani, A.M.A.; Carou, D.; Davim, J.P.; Rubaiee, S.; Ghazali, S. Investigation of Surface Integrity Induced on AZ31C Magnesium Alloy Turned under Cryogenic and Dry Conditions. *Procedia Manuf.* **2019**, *41*, 476–483. [[CrossRef](#)]
28. Kaynak, Y.; Lu, T.; Jawahir, I.S. Cryogenic Machining-Induced Surface Integrity: A Review and Comparison with Dry, MQL, and Flood-Cooled Machining. *Mach. Sci. Technol.* **2014**, *18*, 149–198. [[CrossRef](#)]
29. Danish, M.; Ginta, T.L.; Habib, K.; Abdul Rani, A.M.; Saha, B.B. Effect of Cryogenic Cooling on the Heat Transfer during Turning of AZ31C Magnesium Alloy. *Heat Transf. Eng.* **2018**, *7632*, 1023–1032. [[CrossRef](#)]
30. Wojtowicz, N.; Danis, I.; Monies, F.; Lamesle, P.; Chieragati, R. The Influence of Cutting Conditions on Surface Integrity of a Wrought Magnesium Alloy. *Procedia Eng.* **2013**, *63*, 20–28. [[CrossRef](#)]
31. Pu, Z.; Outeiro, J.C.; Batista, A.C.; Dillon, O.W.; Puleo, D.A.; Jawahir, I.S. Surface Integrity in Dry and Cryogenic Machining of AZ31B Mg Alloy with Varying Cutting Edge Radius Tools. *Procedia Eng.* **2011**, *19*, 282–287. [[CrossRef](#)]
32. Guo, Y.B.; Salahshoor, M. Process Mechanics and Surface Integrity by High-Speed Dry Milling of Biodegradable Magnesium–Calcium Implant Alloys. *CIRP Ann.* **2010**, *59*, 151–154. [[CrossRef](#)]
33. Davis, B.; Dabrow, D.; Ju, L.; Li, A.; Xu, C.; Huang, Y. Study of Chip Morphology and Chip Formation Mechanism During Machining of Magnesium-Based Metal Matrix Composites. *J. Manuf. Sci. Eng.* **2017**, *139*, 091008. [[CrossRef](#)]
34. Fan, L.; Yan, P.; Chen, S.; Chen, H.; Jiao, L.; Qiu, T.; Wang, X. Optimization of Process Parameters and Performances of Cryogenic Cutting of Magnesium Alloy. *Harbin Gongye Daxue Xuebao/J. Harbin Inst. Technol.* **2022**, *54*, 53–69. [[CrossRef](#)]
35. Koklu, U.; Kayhanlar, H. An Experimental Investigation on Machinability of AZ31B Magnesium Alloy under Dry and Dipped Cryogenic Approaches. *J. Mater. Eng. Perform.* **2022**, *31*, 1285–1296. [[CrossRef](#)]
36. Bogajo, I.R.; Tangpronprasert, P.; Virulsri, C.; Keeratihattayakorn, S.; Arrazola, P.J. A Novel Indirect Cryogenic Cooling System for Improving Surface Finish and Reducing Cutting Forces When Turning ASTM F-1537 Cobalt-Chromium Alloys. *Int. J. Adv. Manuf. Technol.* **2020**, *111*, 1971–1989. [[CrossRef](#)]
37. Wu, T.; Li, T.; Ding, X.; Chen, H.; Wang, L. Design of a Modular Green Closed Internal Cooling Turning Tool for Applications. *Int. J. Precis. Eng. Manuf.—Green Technol.* **2018**, *5*, 211–217. [[CrossRef](#)]
38. Isik, Y. Using Internally Cooled Cutting Tools in the Machining of Difficult-to-Cut Materials Based on Waspaloy. *Adv. Mech. Eng.* **2016**, *8*, 1687814016647888. [[CrossRef](#)]
39. Minton, T.; Ghani, S.; Sammler, F.; Bateman, R.; Fürstmann, P.; Roeder, M. Temperature of Internally-Cooled Diamond-Coated Tools for Dry-Cutting Titanium. *Int. J. Mach. Tools Manuf.* **2013**, *75*, 27–35. [[CrossRef](#)]
40. Zakaria, M.S.; Mustapha, M.; Azmi, A.I.; Ahmad, A.; Danish, M.; Rubaiee, S. Machinability Investigations of AZ31 Magnesium Alloy via Submerged Convective Cooling in Turning Process. *J. Mater. Res. Technol.* **2022**, *19*, 3685–3698. [[CrossRef](#)]
41. Zakaria, M.S.; Mustapha, M.; Azmi, A.I.; Ahmad, A.; Ismail, S.O.; Shuaib, N.A. Effects of Submerged Convective Cooling in the Turning of AZ31 Magnesium Alloy for Tool Temperature and Wear Improvement. *Int. J. Adv. Manuf. Technol.* **2022**, *120*, 3181–3200. [[CrossRef](#)]
42. Koklu, U.; Coban, H. Effect of Dipped Cryogenic Approach on Thrust Force, Temperature, Tool Wear and Chip Formation in Drilling of AZ31 Magnesium Alloy. *J. Mater. Res. Technol.* **2020**, *9*, 2870–2880. [[CrossRef](#)]
43. Wang, H.; Dong, S.; Lv, G. Plastic Deformation Characteristics of an Mg–3Al–1Zn Alloy at Low Temperatures. *Mater. Des.* **2016**, *92*, 143–150. [[CrossRef](#)]
44. Shi, K.; Zhang, D.; Ren, J.; Yao, C.; Huang, X. Effect of Cutting Parameters on Machinability Characteristics in Milling of Magnesium Alloy with Carbide Tool. *Adv. Mech. Eng.* **2016**, *8*, 1687814016628392. [[CrossRef](#)]
45. Poulachon, G.; Moisan, A.; Jawahir, I.S. Tool-Wear Mechanisms in Hard Turning with Polycrystalline Cubic Boron Nitride Tools. *Wear* **2001**, *250*, 576–586. [[CrossRef](#)]
46. Barry, J.; Byrne, G. The Mechanisms of Chip Formation in Machining Hardened Steels. *J. Manuf. Sci. Eng.* **2002**, *124*, 528–535. [[CrossRef](#)]
47. Zhang, F.; Liu, Z.; Mao, P.; Wang, F.; Liu, Y. The Modified Temperature Term on Johnson Cook Model for AZ31 Magnesium Alloy. *Materwiss. Werksttech.* **2018**, *49*, 1040–1052. [[CrossRef](#)]
48. Feng, F.; Huang, S.; Meng, Z.; Hu, J.; Lei, Y.; Zhou, M.; Yang, Z. A Constitutive and Fracture Model for AZ31B Magnesium Alloy in the Tensile State. *Mater. Sci. Eng. A* **2014**, *594*, 334–343. [[CrossRef](#)]
49. Giraud, E.; Rossi, F.; Germain, G.; Outeiro, J. Constitutive Modelling of AZ31B-O Magnesium Alloy for Cryogenic Machining. *Procedia CIRP* **2013**, *8*, 521–526. [[CrossRef](#)]
50. Guo, X.; Liu, G.; Sang, S.; Lin, Q.; Qiao, Y. Characteristics and Surface Serviceability for Cryogenic Milling Mg-1.6Ca-2.0Zn Medical Magnesium Alloy. *J. Funct. Biomater.* **2022**, *13*, 179. [[CrossRef](#)]
51. Yildirim, Ç.V.; Kivak, T.; Sarikaya, M.; Şirin, Ş. Evaluation of Tool Wear, Surface Roughness/Topography and Chip Morphology When Machining of Ni-Based Alloy 625 under MQL, Cryogenic Cooling and CryoMQL. *J. Mater. Res. Technol.* **2020**, *9*, 2079–2092. [[CrossRef](#)]

52. Abed, F.; Abuzaid, W.; Morad, Y. Thermomechanical Response of Mg AZ31 at Different Levels of Temperatures and Strain Rates. *MATEC Web Conf.* **2019**, *304*, 01025. [[CrossRef](#)]
53. Wang, Y.; Li, J.; Liu, K.; Jiang, S.; Zhao, D.; Wang, S.; Yang, Y. Experiment and Numerical Study of Chip Formation Mechanism during Cryogenic Machining of Ti-6Al-4V Alloy. *J. Manuf. Process.* **2022**, *84*, 1246–1257. [[CrossRef](#)]
54. Kannan, S.; Pervaiz, S.; Jahan, M.P.; Venkatraghavan, D.S. Cryogenic Drilling of AZ31 Magnesium Syntactic Foams. *Materials* **2020**, *13*, 4094. [[CrossRef](#)]
55. Liyao, G.; Minjie, W.; Chunzheng, D. On Adiabatic Shear Localized Fracture during Serrated Chip Evolution in High Speed Machining of Hardened AISI 1045 Steel. *Int. J. Mech. Sci.* **2013**, *75*, 288–298. [[CrossRef](#)]
56. Pradhan, S.; Singh, S.; Prakash, C.; Królczyk, G.; Pramanik, A.; Pruncu, C.I. Investigation of Machining Characteristics of Hard-to-Machine Ti-6Al-4V-ELI Alloy for Biomedical Applications. *J. Mater. Res. Technol.* **2019**, *8*, 4849–4862. [[CrossRef](#)]
57. Pu, Z.; Song, G.L.; Yang, S.; Outeiro, J.C.; Dillon, O.W.; Puleo, D.A.; Jawahir, I.S. Grain Refined and Basal Textured Surface Produced by Burnishing for Improved Corrosion Performance of AZ31B Mg Alloy. *Corros. Sci.* **2012**, *57*, 192–201. [[CrossRef](#)]
58. Ilanaganar, E.; Anbuselvan, S. Wear Mechanism Map for Extruded AZ31B Magnesium Alloy. *Int. J. Adv. Chem. Sci. Appl. (IJACSA)* **2017**, *5*, 49–54.
59. Yi, S.; Pe, M.T. Mechanical Behavior and Microstructural Evolution of a Mg AZ31 Sheet at Dynamic Strain Rates. *Acta Mater.* **2010**, *58*, 2988–2998. [[CrossRef](#)]
60. Watanabe, H.; Tsutsui, H.; Mukai, T.; Ishikawa, K.; Okanda, Y.; Kohzu, M.; Higashi, K. Grain Size Control of Commercial Wrought Mg-Al-Zn Alloys Utilizing Dynamic Recrystallization. *Mater. Trans.* **2001**, *42*, 1200–1205. [[CrossRef](#)]
61. Pereira, O.; Rodríguez, A.; Fernández-Abia, A.I.; Barreiro, J.; López de Lacalle, L.N. Cryogenic and Minimum Quantity Lubrication for an Eco-Efficiency Turning of AISI 304. *J. Clean. Prod.* **2016**, *139*, 440–449. [[CrossRef](#)]
62. Srinivasan, N.; Rajenthirakumar, D.; Sridhar, R. Micro-Scaled Plastic Deformation Behavior of Biodegradable AZ80 Magnesium Alloy: Experimental and Numerical Investigation. *Int. J. Adv. Manuf. Technol.* **2019**, *102*, 3531–3541. [[CrossRef](#)]
63. Tekumalla, S.; Ajjarapu, M.; Gupta, M. A Novel Turning-Induced-Deformation Based Technique to Process Magnesium Alloys. *Metals* **2019**, *9*, 841. [[CrossRef](#)]
64. Danish, M.; Rubaiee, S.; Ijaz, H. Predictive Modelling and Multi-Objective Optimization of Surface Integrity Parameters in Sustainable Machining Processes of Magnesium Alloy. *Materials* **2021**, *14*, 3547. [[CrossRef](#)] [[PubMed](#)]
65. Mitchell, J.; Crow, N.; Nieto, A. Effect of Surface Roughness on Pitting Corrosion of AZ31 MG Alloy. *Metals* **2020**, *10*, 651. [[CrossRef](#)]
66. Yousefi, S.; Zohoor, M. Effect of Cutting Parameters on the Dimensional Accuracy and Surface Finish in the Hard Turning of MDN250 Steel with Cubic Boron Nitride Tool, for Developing a Knowledge Based Expert System. *Int. J. Mech. Mater. Eng.* **2019**, *14*, 1. [[CrossRef](#)]
67. Viswanathan, R.; Ramesh, S.; Subburam, V. Measurement and Optimization of Performance Characteristics in Turning of Mg Alloy under Dry and MQL Conditions. *Meas. J. Int. Meas. Confed.* **2018**, *120*, 107–113. [[CrossRef](#)]

Disclaimer/Publisher's Note: The statements, opinions and data contained in all publications are solely those of the individual author(s) and contributor(s) and not of MDPI and/or the editor(s). MDPI and/or the editor(s) disclaim responsibility for any injury to people or property resulting from any ideas, methods, instructions or products referred to in the content.